Int. J. Multiphase Flow Vol. 15, No. 3, pp. 421–431, 1989
Printed in Great Britain.

0301-9322/89 $3.00 + 0.00

SIMULTANEOUS MEASUREMENT OF LIQUID FILM THICKNESS, WALL SHEAR STRESS AND GAS FLOW TURBULENCE OF HORIZONTAL WAVY TWO-PHASE FLOW

Y. HAGIWARA, E. ESMAEILZADEH,† H. TSUTSUI and K. SUZUKI
Department of Mechanical Engineering, Kyoto University, Kyoto 606, Japan

(*Received* 1 *October* 1988; *in revised form* 15 *November* 1988)

Abstract—Wall shear stress, liquid film thickness and streamwise gas velocity are measured simultaneously, respectively, with a hot-film, conductance probe and hot-wire at a fully developed location of air–water wavy two-phase flow in a horizontal tube. A conditional sampling technique is applied to eliminate the effect of wire-wetting on the output signal of the hot-wire anemometer. A gradual decrease and successive rapid increase in the gas velocity are clearly observed just before large wave peaks are detected. Minimum gas velocities caused by several waves are lower than the propagation velocity of each wave. This may suggest the existence of a separation bubble attached to the front of large waves. An increase in the wall shear stress caused by the passing of large waves is also observed.

Key Words: wavy two-phase flow, interfacial waves, wall shear stress, conditional sampling, separation bubble

1. INTRODUCTION

Horizontal annular–wavy two-phase flows are encountered in many mechanical or chemical engineering applications, such as steam generators, condensers and chemical processes. Waves appearing on the liquid film surface and peripheral nonuniformity due to the gravitational force make the flow structure complicated and affect the transport phenomena (Butterworth & Robertson 1977).

Recently, the structure of gas-phase flow turbulence near the gas–liquid interface has been drawing attention. Zilker & Hanratty (1979) pointed out that separation and flow reversal occur on solid wavy walls for wave amplitude/wavelength ratios > 0.0165. They also suggested that the motion of a shear-driven film is actually dominated by form drag. Buckles *et al.* (1984) measured single-phase flow velocity fluctuations in a duct with a solid wavy wall of sinusoidal shape. They demonstrated that separation bubbles occurred near the bottom of the sinusoidal wall. Their results suggest that similar separation bubbles may also appear near the troughs of interfacial waves in the case of annular–wavy two-phase flows. However, there have been few measurements near the gas–liquid interface. In this study, simultaneous measurements of liquid film thickness, wall shear stress and streamwise gas-phase velocity are made for wavy air–water two-phase flow in a horizontal tube using a conductance probe, hot-film and hot-wire, respectively.

2. EXPERIMENTAL APPARATUS AND PROCEDURE

2.1. Apparatus

Figure 1 shows the experimental apparatus. It is the same as that described by Hagiwara (1988). Air was drawn in by a turbo-blower ⑤, passed through the nets ① and the contraction nozzle ② and blown into the test section ⑭. The test section was an acrylic tube of 49.4 mm i.d. and 5930 mm length. The air flow rate was measured with a Pitot tube ⑫ located at the outlet of the contraction nozzle; the velocity was assumed to be uniform over the cross section.

The water, stored in a constant-head tank ⑧, was fed into an air–water mixing section ③ by a pump ⑨. The mixing section consisted of triple annular spaces, as shown in figure 2. Each wall

†On leave from the Department of Mechanical Engineering, Tabriz University, Tabriz, Iran.

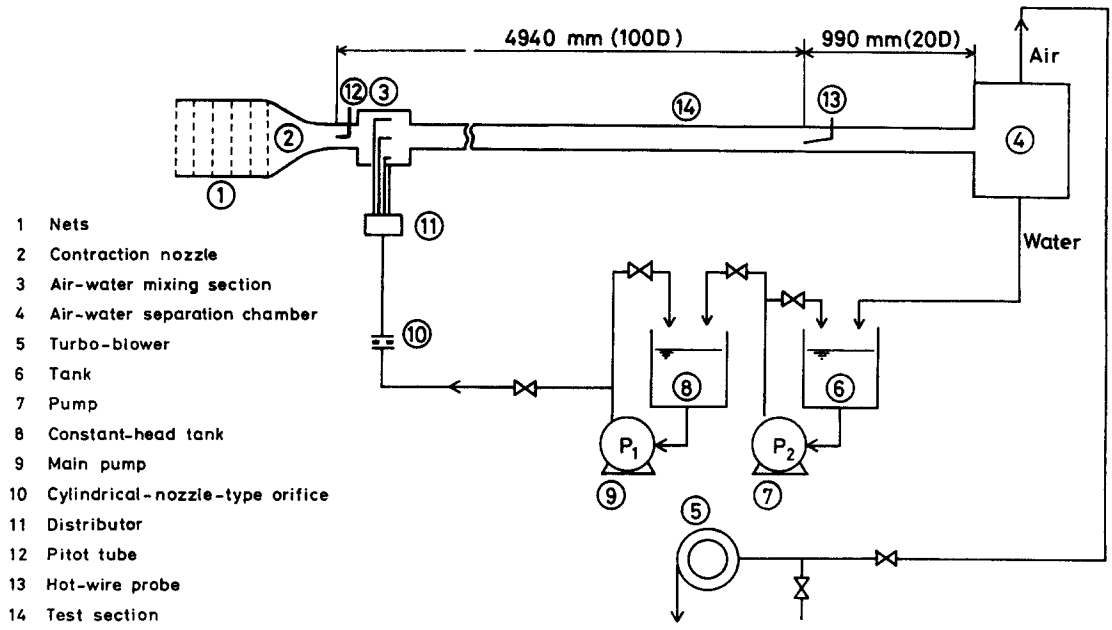

Figure 1. Experimental apparatus.

had a series of holes to supply water to the annular spaces. Numerous small holes in the innermost wall were used to introduce a low-speed uniform injection of water into the air flow. Each annular space of the mixing section was peripherally divided into eight sections and the flow rate into each section was controlled independently in order to establish a non-uniform distribution of the liquid phase within a short distance. The water flow rate was measured with a cylindrical-nozzle-type orifice ⑩ and a manometer. The water separation occurred in a chamber ④ located at the end of the test section.

Figure 3 shows the arrangement of sensors and signal processing circuits used in this experiment. Instantaneous liquid film thickness δ was measured with the conductance probes located at the bottom of the tube at $x = 4940$ and $x = 4965$ mm, where x denotes streamwise distance measured from the outlet of the contraction nozzle. The signal/noise ratio of the output signal of each probe may decrease with the distance l between the two conductance probes because of larger signal interference. On the other hand, identification of corresponding waves in the two signals becomes more difficult as l increases. Compromising these two points, l was set equal to 25 mm. Each probe consisted of a pair of electrodes made of a stainless steel rod of 1.0 mm dia. The end surface of the rod was mounted flush with the inner surface of the tube. The streamwise distance l_e between the two electrodes is 5.0 mm; l_e was determined mainly by ease of manufacture. It had been confirmed

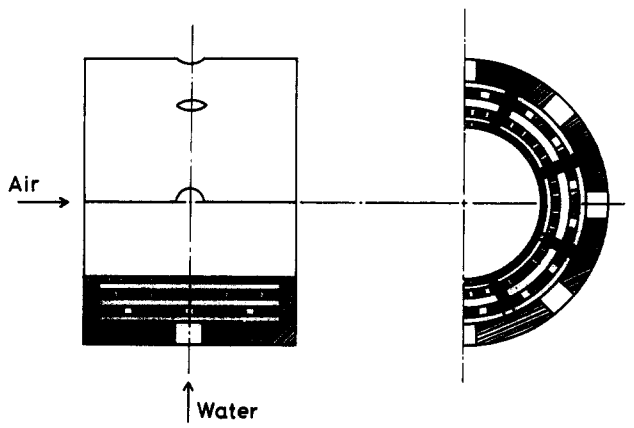

Figure 2. Air–water mixing section.

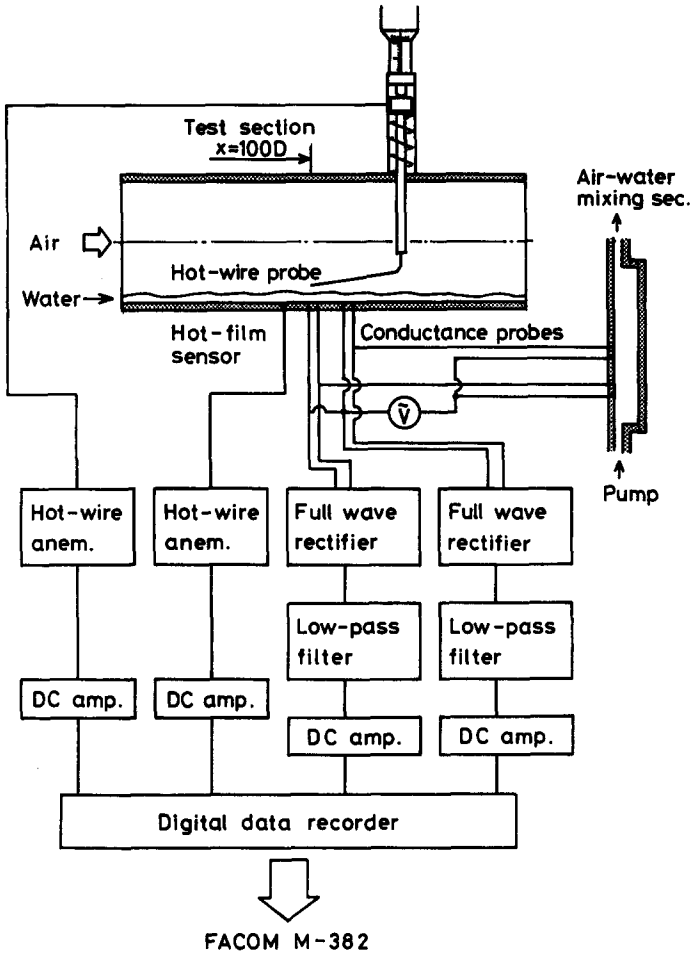

Figure 3. Arrangement of sensors and the signal recording circuit.

that length scale of a small wave is larger than the value of l_e. The probe geometry was nearly the same as that described in the book by Hewitt (1978). A 20 kHz alternating electric current was imposed between the two electrodes of each conductance probe to eliminate the polarizing action of the water. The signal was rectified and was sent to a low-pass filter to produce a signal corresponding to the liquid film thickness. Another two conductance probes were inserted into the water feeding line to compensate for the effect of water properties on the conductance probe reading.

Wall shear stress τ_w was measured with a hot-film sensor (TSI 1268 w) flush-mounted on the test tube inner wall. The hot-film sensor was made of a thin platinum film with dimensions of about 1.0×0.25 mm and coated with a thin layer of epoxy resin. It was located just 17.5 mm upstream from the conductance probe ($x = 4922.5$ mm) oriented with the longer side normal to the main flow direction. The sensor was fixed so that its spanwise center was flush with the inner wall of the test tube, which resulted in the spanwise edge of the sensor being recessed into the wall by 0.01 mm. Lefebvre & LaPointe (1986) concluded from their experimental results that the effect of the recessed edge of their sensor on the instantaneous wall shear stress was negligible. Although the inner diameter of their test tube is almost the same as that in the present study, the diameter of their hot-film sensor is about twice as large as that in the present study. This means that the effect of the recessed edge of the present sensor on the wall shear stress signal is also negligibly small.

The hot-film sensor was operated with a Kanomax 1011 hot-wire anemometer at a low overheat ratio of 1.05 in order to avoid bubble nucleation.

The streamwise gas-phase velocity U_G was measured with an I-type 5 μm hot-wire. The hot-wire was operated with a Kanomax 1011 hot-wire anemometer at an overheat ratio of 1.50. It was traversed radially from the center of the tube to the gas–liquid interface in the plane of $x = 4940$ mm.

The output signal of the hot-wire when positioned very close to the interface was affected by wetting of the wire, which occurred due to its intermittent dipping into some of the larger interfacial waves. The conditional sampling technique developed previously by Hagiwara *et al.* (1982) was used to eliminate the effect of the wire-wetting. When the hot-wire began to be wetted, the value of the velocity signal increased rapidly because of the much better cooling effect in the water. This caused a large value for the time derivative $|dU_G/dt|$ of the streamwise gas velocity signal (see figure 4). Thus, the moment when the time derivative exceeded a certain threshold level was regarded as the beginning of the wetting of the hot-wire. Data in the time period from the beginning to the end of wetting was eliminated from the original sequence of data. The period was determined by a method similar to that developed by Hagiwara *et al.* (1982) for eliminating liquid droplet collision with a hot-wire.

Figure 4 shows the velocity signal, its time derivative and the simultaneously obtained liquid film thickness. When the film thickness is so great that the hot-wire lies below the interface, the wire should be wetted. However, the time duration of wire-wetting obtained from the film thickness time trace is found in the figure to be longer than that estimated from the time derivative of velocity signal. But this is not unreasonable if the spatial resolution of the liquid film thickness measurement is taken into account. The film thickness measured was the average of the film thickness between the two electrodes located 5.0 mm apart in streamwise direction. Therefore, its signal exhibits a wider skirt than the actual geometry of the waves.

The output signals from the anemometers were attenuated with DC amplifiers, and were digitized together with the signal of the liquid film thickness at 4 kHz. These signals were recorded simultaneously on digital magnetic tape with a TEAC DR2000 digital data recorder. The recorded signal incorporates errors caused by the digitization and signal attenuation with the DC amplifier. The digitization of the data causes an error of about 2.3% in the wall shear stress and the streamwise gas velocity. The total magnitude of the error, including those caused by the signal processing with the calibrated curve, was estimated to be about 5% in these signals. The digitized data were processed using a FACOM M382 computer at the Data Processing Center, Kyoto University.

2.2. Calibration of the sensors

Prior to the experiment, calibration was done for the output signal of the hot-film sensor. It is known that the relationship between the output voltage E from the hot-wire anemometer and the wall shear stress τ_w is given by the following equation:

$$E^2 = a + b\tau_w^{1/3}, \qquad [1]$$

where the constants a and b are determined by calibration. For the calibration we used the laminar flow in an annulus with 0.70 mm clearance. The annulus was realized by inserting a rod of 48.0 mm dia into the test tube which had been removed from the test loop. Stainless steel balls

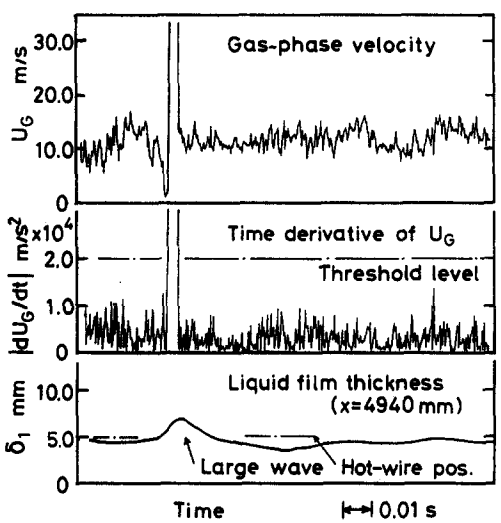

Figure 4. Wire-wetting effect.

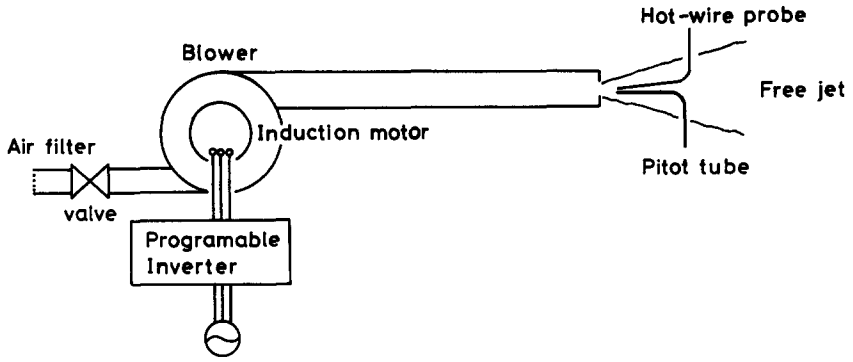

Figure 5. Calibration flow for the hot-wire.

of 0.70 mm dia were attached to the surface of the rod as spacers at every 90° circumferentially in planes of every 200 mm streamwise distance. It had been confirmed with a flow visualization technique that the spacer disturbed the calibration flow only in a small region close to the spacer. This means that the calibration flow was essentially laminar and circumferentially uniform.

The wall shear stress τ_w in [1] was calculated analytically from the fully developed laminar velocity distribution in the annulus. The output voltage E from the anemometer was recorded on magnetic tape and processed by computer in the same manner as that of the measurement mentioned above. In the calibration we changed the flow rate through the annulus in the laminar flow regime, where the maximum Reynolds number based on the hydraulic equivalent diameter as a length scale was 2100. Constants a and b were finally determined by applying the least-square method to the obtained values of E^2 and τ_w.

It was confirmed by another calibration that the relationship between the output voltage E of the hot-wire and the gas velocity U_G can be expressed by the following equation:

$$E^2 = c + dU_G^{0.5}. \quad [2]$$

This equation was put forward by King (1914) and the constants c and d were to be determined by calibration. The calibration was done using the device shown in figure 5. Air was blown into a tube by a blower and was issued as a free jet from the hole at the end of the tube. The potential core region of the free jet was used for the calibration flow. The uniform velocity U_G of the potential core was measured with a Pitot tube and a manometer, while the output voltage E from the anemometer was recorded on magnetic tape and processed by computer in the same manner as that of the wall shear stress calibration. The constants c and d were determined in the same way as constants for a and b.

Direct calibration of the conductance probe was impossible. However, the following indirect calibration was performed. First, the non-linear relationship between the probe output signal and the film thickness was measured for a probe of similar geometry in a rectangular duct with variable space in the range 0.6–6.0 mm.† The calibration curve obtained was used as the one for the probe located in the test section. Secondly, a liquid flow of 0.70 mm depth was formed in the test tube, as will be discussed later, and the output signals from the probes were recorded. The film thickness evaluated with the applied calibration curve from the recorded signal was confirmed to agree with the actual thickness within 8% accuracy.

2.3. Flow visualization technique

Supplemental flow visualization was performed using tufts to observe gas-phase flow behavior near the interface. The tufts were made of many fine silk strings of about 20 μm dia, 5.5 mm length. The tufts were fixed at the edge of fine rod of 1.0 mm dia. The rod was traversed radially from the center of the test tube to the interface by a micrometer, which is similar to that shown in figure 3. The strings entwine around each other via wetting, when the tufts are located near the interface. To avoid this, the surface of the strings was covered with polymer solution.

†The liquid film thickness δ occasionally exceeded 6.0 mm when the crests of large waves reached the detection point. The value of δ was estimated in such cases by linear extrapolation of calibration curve. This causes some degree of errors in the value of δ, but it is estimated to be very small because the relationship between δ and the probe output signal in the range 4.0–6.0 mm is expected to be almost linear in the calibration curve.

The tufts can follow unsteady flows only in a low frequency range (see Nakaguchi 1977). The characteristic response time of tufts to gas flow fluctuation was checked by using unsteady free jet flow. The unsteady jet was realized by changing the rpm value of the induction motor shown in figure 5 with an inverter. The frequency of the fluctuation can be chosen over the range of 1–7 Hz using the inverter. The response time thus determined was 4 Hz.

2.4. Experimental conditions

The superficial gas velocity $j_G = 14$ m/s (gas Reynolds number $Re_G = 4.0 \times 10^4$) in the present study, which means the gas flow is turbulent. Three different superficial liquid velocities $j_L = 0.0061$ m/s (liquid Reynolds number $Re_L = 300$), $j_L = 0.010$ m/s ($Re_L = 500$) and $j_L = 0.020$ m/s ($Re_L = 1000$), are chosen. Liquid flows as a film, formed only near the bottom of the test tube, and the interface was covered with waves; i.e. wavy two-phase flow. The above flow rate conditions all lie in the "wavy flow" region of several flow regime maps presented by Mandhane *et al.* (1974) and Ebner *et al.* (1987) among others.

3. RESULTS AND DISCUSSION

3.1. Radial velocity distribution in the gas phase

Figures 6(a, b) show radial distributions of the mean streamwise velocity and the longitudinal turbulence intensity $\sqrt{\overline{u_G'^2}}$ of the gas-phase flow plotted against the vertical distance y from the tube bottom. The velocity signal very close to the interface was subject to the effect of the wire-wetting.

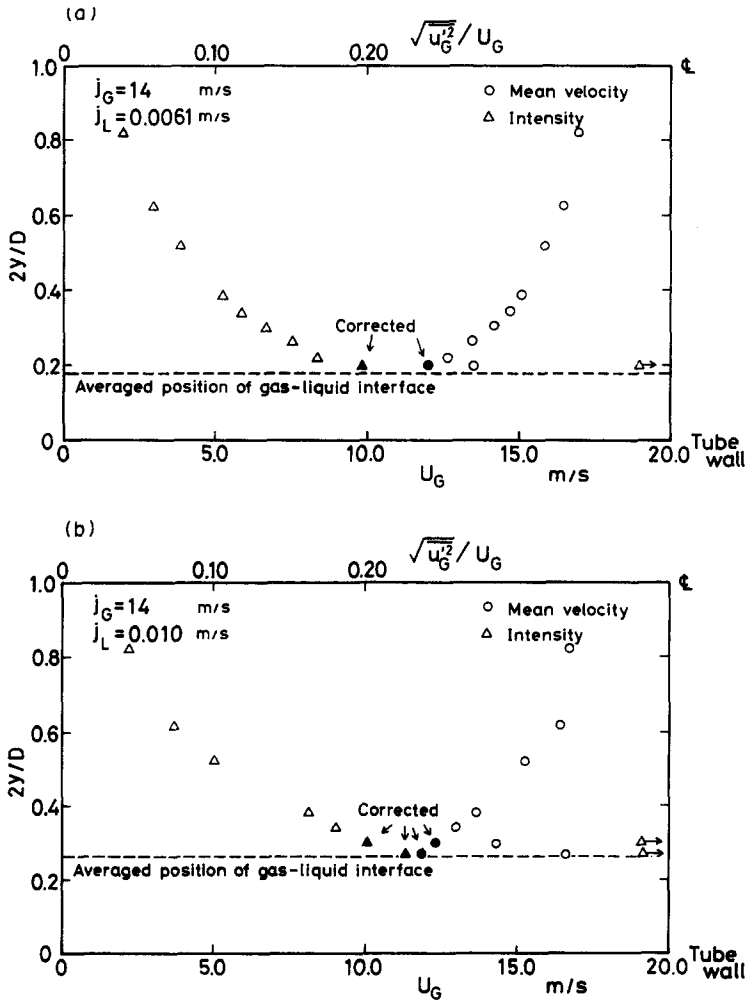

Figure 6. Radial distribution of the mean velocity and the turbulence intensity of gas-phase flow: (a) $j_L = 0.0061$ m/s; (b) $j_L = 0.01$ m/s.

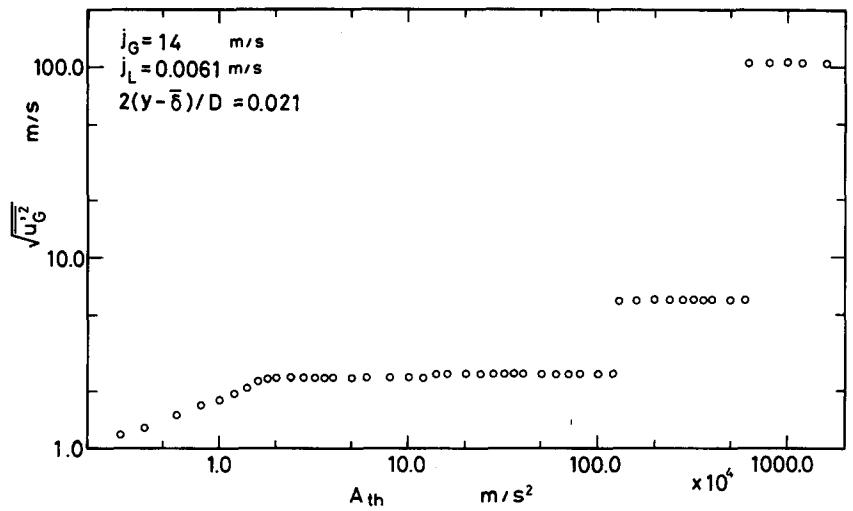

Figure 7. Gas-phase flow turbulence intensity obtained with various values of the threshold level.

To eliminate this effect, a conditional sampling technique was used. A threshold for the time derivative of the signal was introduced to distinguish the signal under the wetting effect from the intrinsic turbulent fluctuation. Figure 7 shows the plot of the standard deviation of the longitudinal velocity (i.e. streamwise turbulence intensity) obtained with various levels of the threshold A_{th}. When A_{th} is small, not only the wetting portion of the hot-wire but also large fluctuations in the gas velocity were eliminated from the signal. Therefore, the value of $\sqrt{u_G'^2}$ becomes smaller than the genuine value. On the other hand, if A_{th} is too large, some wetting phenomena cannot be eliminated and the measured value of $\sqrt{u_G'^2}$ includes serious errors. To eliminate the wetting effect properly, a relatively smaller value of A_{th} was preferred. Taken from figure 7, A_{th} was set equal to 2.0×10^4 m/s^2 in the present study. The period for which the data should be eliminated from the original sequence of data was determined to be 2.03 ms, which is about twice as long as the value estimated in the previous study. This is mainly due to the fact that the duration of wetting by an interfacial wave is longer than that by a small droplet.

The corrected value of the mean streamwise gas velocity obtained with the above A_{th} is also plotted in figures 6(a, b). After the correction is made, the distribution of the mean velocity is found to be smooth in shape and similar to that for single-phase flow. The results for the longitudinal turbulence intensity are also quite similar to the experimental results for single-phase flow of Laufer (1953).

3.2. Time series of the signals

Near the interface, a remarkable correspondence was clearly obtained between the gas flow velocity variation with time and the propagation of the large two-dimensional wave, as seen in figures 8(a, b). The hot-wire was located 0.51 mm distant from the averaged interface position. A gradual decrease followed by a rapid increase in the gas velocity can be observed clearly just before the peak of the large two-dimensional wave is detected. It was found that the instantaneous minimum value of U_G was reduced to only 5–10% of its time-mean value.

Figures 9(a, b) show the comparison of the minimum gas velocity U_{Gmin} caused by the large wave with the propagation velocity C of the large wave. The propagation velocity was estimated from the time difference between the corresponding crests which appeared in the output signals of the two conductance probes, taking account of the distance between the two probes. The output signals of the conductance probes do not differ remarkably from each other, which means the large wave propagates without significantly changing its configuration in the short distance between the two conductance probes. This was also confirmed by visual observation. The front of the large wave, therefore, may propagate with the same velocity as that of the wave crest. The open circles in the figure mean that the hot-wire dipped into the wave just after the minimum gas velocity had been detected by the wire, the solid circles signify that the wave passed below the hot-wire. About half of the total number of values of the minimum velocity U_{Gmin} are higher than the propagation

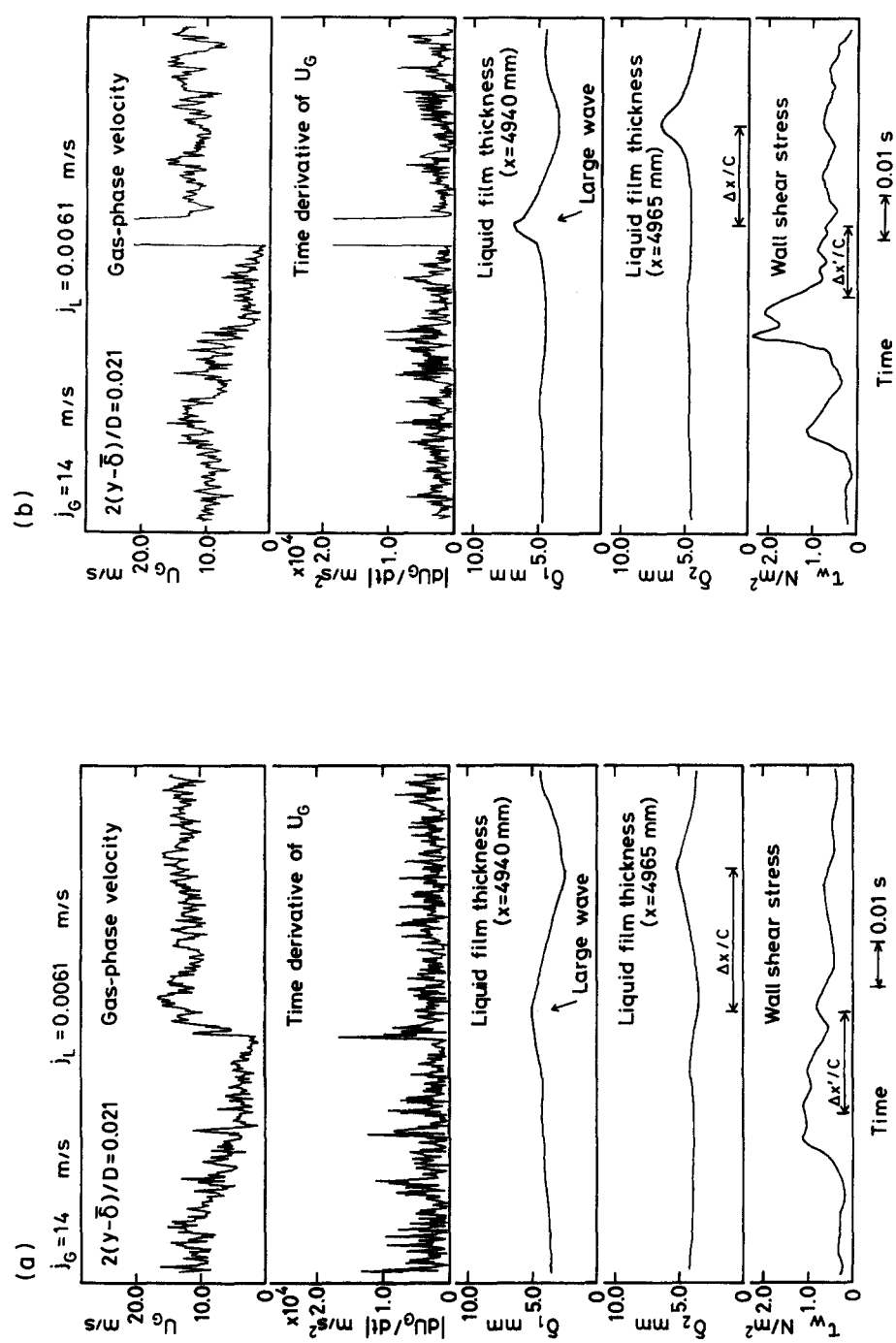

Figure 8. Signals of the gas-phase velocity, its time derivative, liquid film thickness and wall shear stress: (a) without wire-wetting; (b) with wire-wetting.

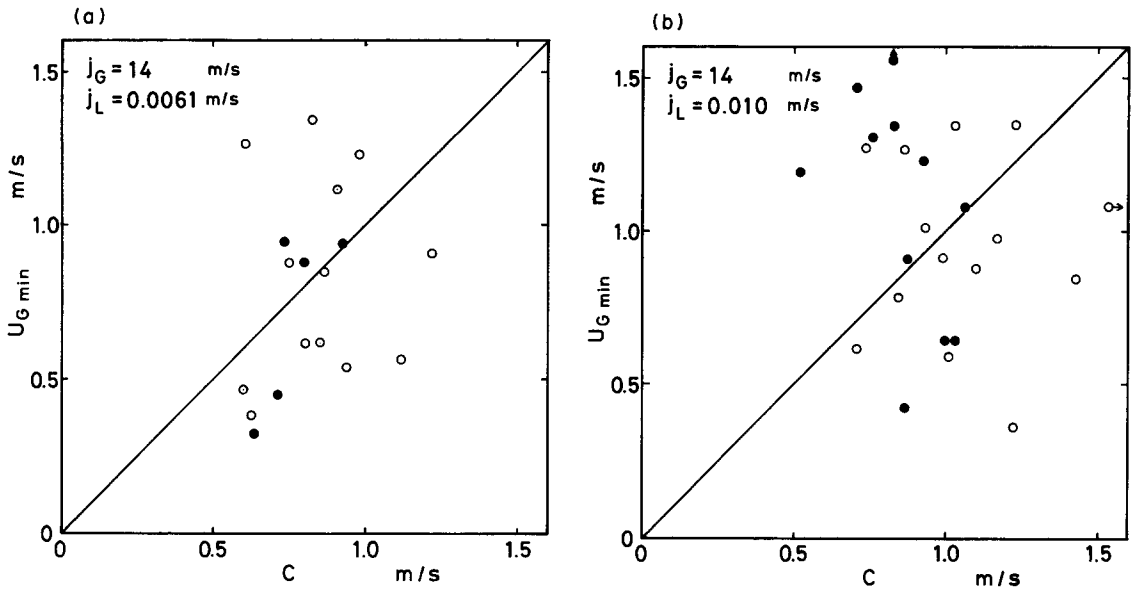

Figure 9. Comparison of the minimum gas velocity with the wave propagation velocity: (a) $j_L = 0.0061$ m/s, $2(y-\delta)/D = 0.021$; (b) $j_L = 0.01$ m/s, $2(y-\delta)/D = 0.046$.

velocity of the corresponding wave regardless of its height. This means that gas flows along the waves with a greater velocity than that of the interface. The other values of U_{Gmin}, however, are clearly lower than those of the corresponding wave propagation velocity. This indicates that recirculating flow should have been observed in front of the waves by an observer moving with the wave propagation velocity. This was not observed at positions a little bit farther from the interface.† This result suggests the existence of separation bubbles formed in the front region of several large waves.

As mentioned above, the hot-film sensor was located 17.5 mm upstream from the location of the hot-wire and the upstream conductance probe. Considering the sensor distance and the measured wave propagation velocity, the maximum wall shear stress shown in figures 8(a, b) is found to correspond to the passing of the large two-dimensional wave. A similar correspondence was observed between the peaks of τ_w and δ for the passing of all the large waves examined.

3.3. Flow visualization near the interface

Gas-phase flow near the interface was visualized with the tuft probe. Figures 10(a, b) show a typical example of photographs of the tuft probe and the interfacial waves. Figure 10(a) shows the instant when only ripple waves appear and figure 10(b) shows the moment when a large wave also approaches the tufts. In figure 10(a), the fact that the ends of the tufts are pointing downstream indicates that the gas velocity is high even near the interface. On the other hand in figure 10(b), the tufts located at the same positions as in figure 10(a) tend to point to the interface. The bright area in the photograph was caused by the scattering of light at the deformed interface of the large two-dimensional wave so its existence shows that the large wave was approaching the tuft position. This suggests that remarkable velocity retardation occurs in front of the wave. This confirms qualitatively the variation of the gas velocity in front of the wave discussed above.

†The dimensionless form of the vertical distance Δy between the wave trough and the hot-wire for each wave was defined as follows:

$$\Delta y^+ = \Delta y \frac{\sqrt{\tau_i/\rho_G}}{\nu_G}$$

where τ_i is the interfacial shear stress [estimated by the theory of Taitel & Dukler (1976)], ρ_G is the gas density and ν_G is the gas kinematic viscosity. Almost all the points representing $U_{Gmin} < C$ in figure 9(a) have values of $\Delta y^+ < 60$. This suggests that reversed flow relative to the wave motion caused by the recirculation is restricted in the region very close to the wave trough.

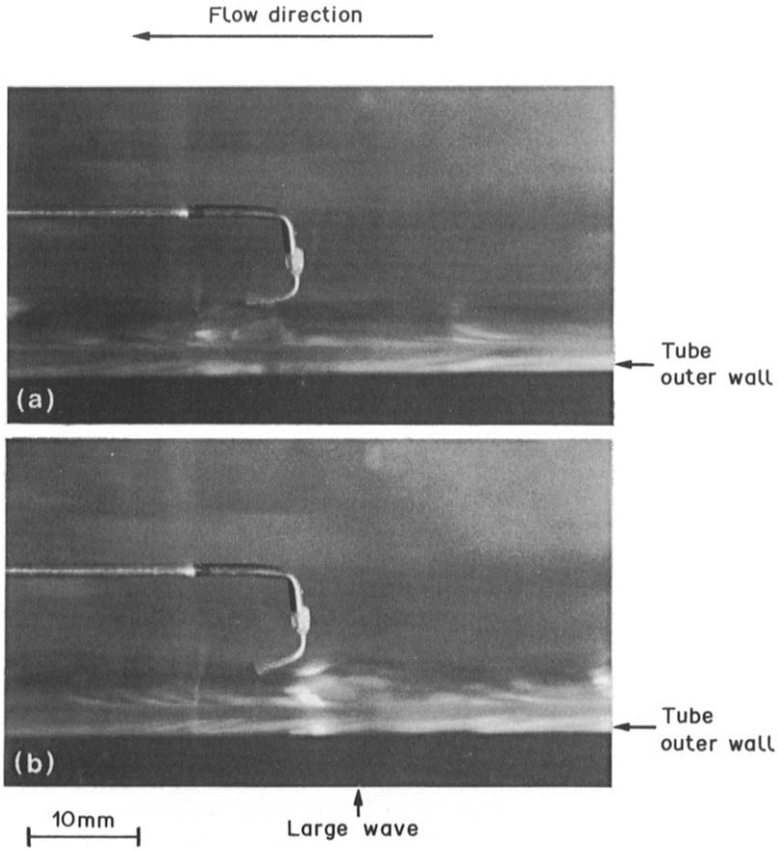

Figure 10. Interfacial waves and tufts: (a) ripple wave; (b) large wave.

4. CONCLUSIONS

Simultaneous measurements were performed on liquid film thickness, wall shear stress and streamwise gas velocity for the wavy air–water two-phase flow in a horizontal tube. A gradual decrease followed by a rapid increase in the streamwise gas velocity was clearly observed just before the front of the large wave was detected. This may suggest the existence of a separation bubble formed in the region in front of the large wave. It was also observed that the large wave causes an increase in the wall shear stress. A conditional sampling technique was applied in order to eliminate the wetting effect of the hot-wire from the output signal. The corrected distributions of the mean gas velocity and longitudinal turbulence intensity were similar to those for single-phase flow.

Acknowledgements—The authors are very grateful to Y. Sumitomo and K. Seki for developing the experimental method.

REFERENCES

BUCKLES, J. J., HANRATTY, T. J. & ADRIAN, R. J. 1984 Separated turbulent flow over a small amplitude wave. In *Proc. 2nd Int. Symp. on Applications of Laser Anemometry to Fluid Mechanics*, Paper 15.4.

BUTTERWORTH, D. & ROBERTSON, J. M. 1977 Boiling and flow in horizontal tubes. In *Two-phase Flow and Heat Transfer*, Chap. 11 (Edited by BUTTERWORTH, D. & HEWITT, G. F.). Oxford Univ. Press, Oxford.

EBNER, L., DRAHOŠ, J., EBNER, G. & ČERMÁK, J. 1987 Characterization of hydrodynamic regimes in horizontal two-phase flow. Part I: pressure drop measurements. *Chem. Engng Process.* **22,** 39–43.

HAGIWARA, Y. 1988 Experimental studies on chaotic behaviour of liquid film flow in annular two-phase flows. *PhysicoChem. Hydrodynam.* **10,** 135–147.

HAGIWARA, Y., SUZUKI, K. & SATO, T. 1982 Continuous phase flow behaviour of a mist flow in a circular tube. *Trans. Jap. Soc. mech. Engrs* **48B,** 1120–1127. In Japanese.

HAGIWARA, Y., SUZUKI, K., SATO, T. & CHIGUSA, N. 1983 Simultaneous measurements of wall shear stress and liquid film thickness in an annular-mist two-phase flow in a vertical tube. *Proc. ASME–JSME therm. Engng Joint Conf.* **1,** 55–62.

HEWITT, G. F. 1978 *Measurement of Two-phase Flow Parameters.* Academic Press, London.

KING, L. V. 1914 On the convection of heat from small cylinders in a stream of fluid: determination of the convection constants of small platinum wires with applications to hot-wire anemometry. *Phil. Trans. R. Soc.* **214A,** 373–432.

LAUFER, J. 1953 The structure of turbulence in fully developed pipe flow. NACA Report 1174, pp. 417–434.

LEFEBVRE, P. J. & LAPOINTE, K. M. 1986 The effect of mounting position on hot-film wall shear stress sensors. Paper AIAA 86-1101.

MANDHANE, J. M., GREGORY, G. A. & AZIZ, K. 1974 A flow pattern map for gas–liquid flow in horizontal pipes. *Int. J. Multiphase Flow* **1,** 537–553.

NAKAGUCHI, H. 1977 Tuft method. In *Handbook of Flow Visualization,* Chap. 4 (Edited by ASANUMA, T.). Asakura Book Co., Tokyo. In Japanese.

TAITEL, Y. & DUKLER, A. E. 1976 A model for predicting flow regime transitions in horizontal and near horizontal gas–liquid flow. *AIChE Jl* **22,** 47–55.

ZILKER, D. P. & HANRATTY, T. J. 1979 Influence of the amplitude of a solid wavy wall on a turbulent flow. Part 2. Separated flows. *J. Fluid Mech.* **90,** 257–271.